

Hydrothermal synthesis, characterization and luminescence properties of orange–red-emitting phosphors SnO₂:Eu

Yongqing Zhai¹ · Qian Zhao¹ · Ying Han¹ · Meng Wang¹ · Jiabao Yu¹

Received: 30 June 2015 / Accepted: 27 September 2015 / Published online: 5 October 2015
© Springer Science+Business Media New York 2015

Abstract Orange–red-emitting phosphors SnO₂:Eu nanoparticles were synthesized by hydrothermal method followed by calcination process. The phase structure, morphology, optical absorption and luminescence properties of the obtained samples were characterized by X-ray powder diffraction, scanning electron microscopy, UV–Vis optical absorption spectra and photoluminescence spectra. The results indicated that the as-synthesized SnO₂:Eu was all tetragonal phase with space group P42/mnm when pH = 1. The particles were nearly spherical in shape, and the average size was about 100 nm. The excitation spectrum was composed of a broad band ascribed to the direct optical transition from the valence band to the conduction band of SnO₂. The emission spectrum was consisted of a strong peak and several weak peaks, and the main peak was at 589 nm, corresponding to the ⁵D₀ → ⁷F₁ magnetic dipole transition of Eu³⁺. The SnO₂:xEu phosphors presented excellent orange–red-emitting properties when the concentration (x) of Eu³⁺ was 0.09, pH = 1, calcination temperature and time were 900 °C and 3 h, respectively.

1 Introduction

Tin oxide (SnO₂) is a n-type semiconductor with a wide band gap (E_g = 3.6 eV, at 300 K) and it has been widely used in gas sensors [1], dye-based solar cells [2], pho-

todetectors [3] and catalysts [4] due to its good physical and chemical stability, electrical, optical and ferromagnetic properties [5]. Also, SnO₂ is an excellent host material for rare-earth ions. Zhang et al. [6] synthesized SnO₂:Sm³⁺, Zr⁴⁺ afterglow phosphor by solid state reaction. Pillai et al. [7] adopted chemical co-precipitation method to obtain Dy³⁺-doped nano-crystalline SnO₂ and discussed its luminescent property.

Recently, Eu³⁺ doped SnO₂ phosphors has attracted much attention because of its efficient reddish-orange emitting and potential applications in thin film electroluminescent (TFEL) devices, cathodoluminescent devices and luminescent labels [8]. However, there are still some problems for the synthesis of SnO₂:Eu phosphors. One is that it's difficult for Eu³⁺ to enter into SnO₂ lattice due to the difference in radius and charge between Sn⁴⁺ and Eu³⁺ [9], which will lead to inefficient energy transfer and poor luminescent emission. The other problem is that high concentration of Eu³⁺ will result in the formation of impurity phase Eu₂Sn₂O₇ [10], which can be another hinder for efficient luminescent emission.

In this work, pure phase SnO₂:Eu samples were successfully synthesized by hydrothermal method followed by calcination process. The hydrothermal route was selected to obtain homogeneous spherical particles with good dispersion, and the calcination process was used to accelerate the Eu³⁺ entering into the host lattice and promote the crystallinity of the sample, furthermore, improve the luminescent intensity. The possible energy transfer mechanism of SnO₂:Eu system was discussed. The effects of pH of the solution, calcination temperature, calcination time and doping concentration of Eu³⁺ on the phase structure and luminescent properties of SnO₂:Eu phosphors were investigated in detail.

✉ Yongqing Zhai
zhaiyongqinghbu@163.com

¹ College of Chemistry and Environmental Science, Hebei University, Baoding 071002, China

2 Experimental

2.1 The preparation of $\text{SnO}_2\cdot\text{Eu}$ samples

$\text{SnCl}_2\cdot 2\text{H}_2\text{O}$, $\text{C}_4\text{H}_6\text{O}_6\cdot 2\text{H}_2\text{O}$, $\text{Eu}(\text{NO}_3)_3$, NaOH and $\text{C}_2\text{H}_5\text{OH}$ were used as raw materials. They were all analytical reagents (AR) and were used directly without further purification. $\text{Eu}(\text{NO}_3)_3$ aqueous solutions were obtained by dissolving Eu_2O_3 in dilute HNO_3 solution under heating with agitation. The laboratory water is deionized water.

The $\text{SnO}_2\cdot\text{Eu}$ samples were synthesized by hydrothermal method and the procedure is as follows. Firstly, 3 g $\text{C}_4\text{H}_6\text{O}_6\cdot 2\text{H}_2\text{O}$ was dissolved in 40 mL deionized water, then a certain amount of $\text{Eu}(\text{NO}_3)_3$ aqueous solution and $\text{SnCl}_2\cdot 2\text{H}_2\text{O}$ according to the stoichiometric ratio of target product $\text{SnO}_2\cdot x\text{Eu}$ ($x = 0.03, 0.05, 0.07, 0.09, 0.11$) were added to the above solution under magnetic stirring to form clear solution. Subsequently, NaOH solution (4 mol/L) was dropped into the stirred solution to adjust the pH value to 1 or 3. Next, the mixture was transferred into a 100 mL Teflon-lined stainless steel autoclave, and the suitable amount of deionized water was added to reach to a filling capacity of 75 %. The autoclave was sealed, and heated at 200 °C for 12 h in a oven. After air-cooled to room temperature, the precipitate was centrifuged, and washed three times with deionized water and absolute ethanol, respectively, then dried at 90 °C. Finally, the obtained powders were calcined at different temperature ($T = 700, 800, 900$ or 1000 °C) for a period of time ($t = 1, 3$ or 5 h) in the air.

2.2 Characterization

Phase structure of synthesized samples were analyzed by a D8 Advance X-ray powder diffraction (XRD) with $\text{Cu-K}\alpha$ radiation ($20^\circ \leq 2\theta \leq 80^\circ$, $\lambda = 0.1540600$ nm, 40 kV \times 40 mA). The particle size and morphology of the samples were characterized with scanning electron microscopy (SEM). UV–Vis absorption spectra were obtained using TU-1901 double beam UV–Vis spectrophotometer. The photoluminescence spectra (PL) were recorded on an F-380 fluorescence spectrophotometer with Xe lamp as excitation source, the test conditions were as follows. The excitation and emission slit were 10 and 5 nm, respectively, the voltage was 430 V and gain was “2”. All measurements were performed at room temperature.

3 Results and discussion

3.1 Phase structure of the samples

To study the phase structure of the synthesized samples under different conditions, XRD analysis was carried out.

Figure 1 shows the XRD patterns of samples prepared with different pH value of the solution ($x = 0.09$, $T = 900$ °C and $t = 3$ h). From Fig. 1, it can be seen that when $\text{pH} = 1$, all the peaks are indexed to pure tetragonal rutile phase SnO_2 with space group $\text{P}42/\text{mnm}$, which agrees well with the standard card (JCPDS NO. 41-1445). However, when $\text{pH} = 3$, the intensity of diffraction peaks corresponding to SnO_2 obviously decreases, and two weak peaks assigned to the impurity phase $\text{Eu}_2\text{Sn}_2\text{O}_7$ (JCPDS NO. 13-0182) appears. The reasonable explanation is that with pH value increasing, the acidity of solution decreases, which can accelerate the hydrolysis of Sn^{2+} to form $\text{Sn}(\text{OH})_2$ leading to the increase of nucleation rate during the subsequent hydrothermal reaction. While increasing nucleation rate is not beneficial for crystal growth, which means poor crystallinity. Also, the appearance of impurity phase $\text{Eu}_2\text{Sn}_2\text{O}_7$ may be related to the existing form of Eu^{3+} at different pH values. When the pH is increased to 3, some of Eu^{3+} ions are hydrolyzed to form $\text{Eu}(\text{OH})_3$, and it can further react with $\text{Sn}(\text{OH})_4$ [the oxidation product of $\text{Sn}(\text{OH})_2$] which is a kind of amphoteric hydroxide, to produce $\text{Eu}_2\text{Sn}_2\text{O}_7$ under hydrothermal condition. Therefore, pH of the solution should be adjusted to 1 in order to obtain the pure phase SnO_2 .

Figure 2 presents the XRD patterns of samples calcinated at different temperature ($x = 0.09$, $\text{pH} = 1$ and $t = 3$ h). It can be observed that the samples obtained in the range of 700–1000 °C are all pure tetragonal phase SnO_2 . Calcination temperature has great effect on the intensity of diffraction peaks. From 700 to 900 °C, the intensity of peaks is significantly enhanced, which means that the crystallinity of the samples is improved greatly with the increase of calcination temperature. It's calculated by Scherrer formula [11] that the grain size of samples is 26, 37 and 40 nm corresponding to 700, 800 and 900 °C.

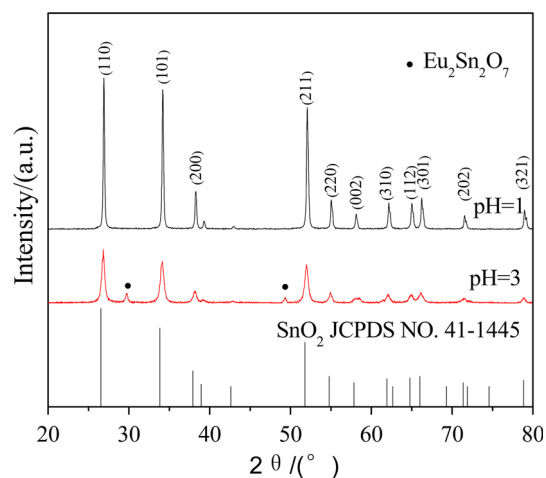


Fig. 1 XRD patterns of samples synthesized at different pH values

Nevertheless, when the temperature is up to 1000 °C, the peak intensity of the sample becomes weak slightly and the calculated grain size is 38 nm. The reason is that higher temperature may induce the formation of oxygen vacancy defects, which will lead to poor crystallinity. Through the above analysis, the appropriate calcination temperature is confirmed to 900 °C in order to obtain the pure tetragonal phase SnO₂:Eu with high crystallinity.

The XRD patterns of samples calcinated for different time ($x = 0.09$, pH = 1 and $T = 900$ °C) are shown in Fig. 3. It can be seen that as the calcination time is prolonged, the intensity of diffraction peaks increases as well as the crystallinity of samples. But the intensity of peaks is not enhanced obviously when $t = 5$ h contrasted with that of the sample obtained under $t = 3$ h. Taking into account of the energy savings, 3 h is chosen as the suitable calcination time.

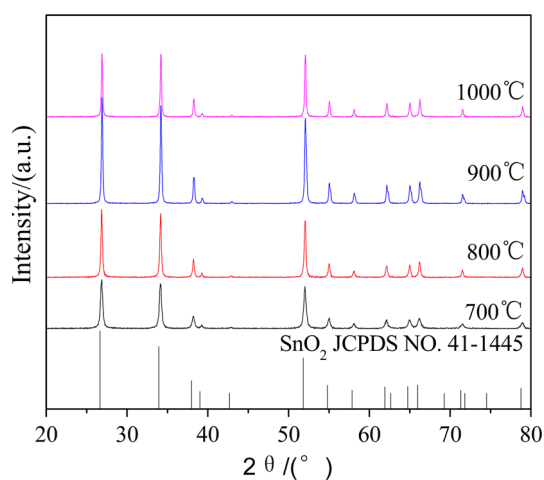


Fig. 2 XRD patterns of samples calcinated at different temperatures

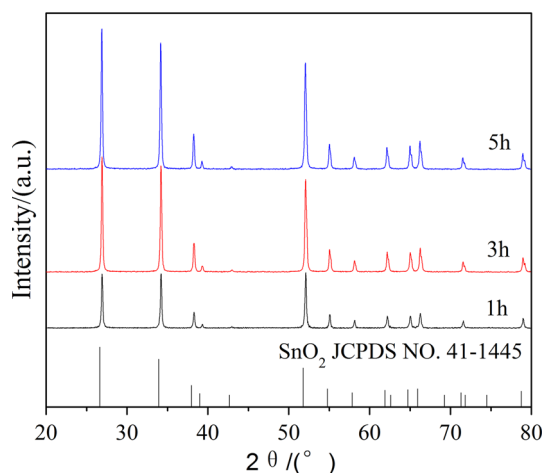


Fig. 3 XRD patterns of samples synthesized under different calcination time

Figure 4 shows the XRD patterns of samples synthesized with different Eu³⁺ concentration (pH = 1, $T = 900$ °C and $t = 3$ h). As seen in Fig. 4, all peaks can be indexed to tetragonal phase SnO₂. Even when x is up to 0.11, no impurity phase of Eu appears. Psuja et al. [10] used modified Pechini method to synthesize SnO₂:Eu nanopowders and the XRD analysis result indicated that the impurity phase Eu₂Sn₂O₇ appeared when Eu³⁺ concentration was above 2 mol%. Thus, the high doping concentration of Eu³⁺ can be achieved by our present synthesis method. From Fig. 4, it can be also observed that with the increase of x , the intensity of peaks becomes weaker, which suggests that Eu³⁺ has entered into SnO₂ lattice. The reason is that the ionic radius of Eu³⁺ (0.095 nm) is larger than that of Sn⁴⁺ (0.069 nm), so the incorporation of Eu³⁺ causes expansion and distortion of the host lattice, and the unequivalent substitution between Eu³⁺ and Sn⁴⁺ can induce the generation of oxygen vacancies [12], which results in the crystallinity decreases.

3.2 Morphology of the samples

The SEM images of samples synthesized with different calcination time are shown in Fig. 5. It can be seen that the particles are nearly spherical in shape and the size is 70–100 and 90–120 nm for 1 and 3 h, respectively.

3.3 Mechanism analysis of the hydrothermal synthesis

In the present work, SnCl₂·2H₂O was used to provide Sn²⁺. Tartaric acid was used as complexing agent to increase the solubility of SnCl₂·2H₂O in water, meanwhile it could also inhabit the hydrolysis of SnCl₂·2H₂O. Sn²⁺ from

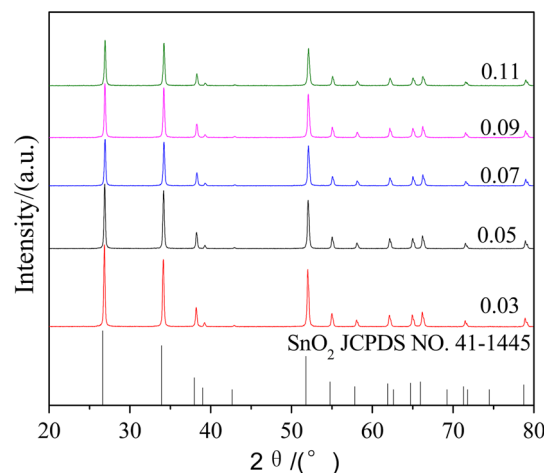


Fig. 4 XRD patterns of samples obtained with different Eu³⁺ concentrations x

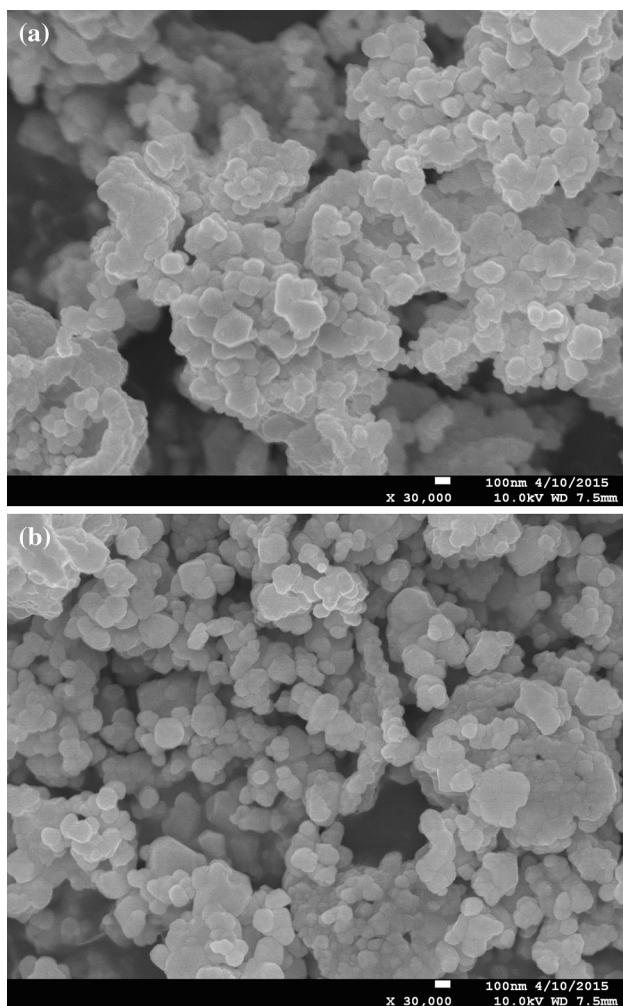
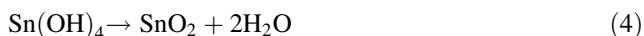
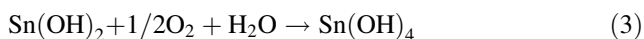
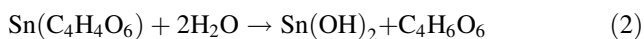
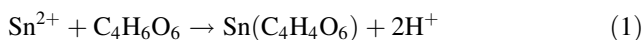


Fig. 5 SEM images of $\text{SnO}_2:\text{xEu}$ ($x = 0.09$) samples calcinated for a 1 h; b 3 h

$\text{SnCl}_2 \cdot 2\text{H}_2\text{O}$ reacted with tartaric acid to form the soluble $\text{Sn}(\text{C}_4\text{H}_4\text{O}_6)$. So the solution was transparent. During the hydrothermal reaction, the high temperature and pressure conditions could provide enough energy to accelerate $\text{Sn}(\text{C}_4\text{H}_4\text{O}_6)$ to hydrolyze and form $\text{Sn}(\text{OH})_2$. $\text{Sn}(\text{OH})_2$ was unstable and could be oxidized to $\text{Sn}(\text{OH})_4$ by residual oxygen in the solution together with the water. Then the dehydration of $\text{Sn}(\text{OH})_4$ resulted in the formation of SnO_2 nanocrystals.

The chemical reactions involved may be as follows:



Since the molecular oxygen dissolved in the solution was less, the reaction (3) was very slow and became the rate-determining step of the whole process. With SnO_2

precipitation generating, all the reactions proceeded to the right, thus the $\text{Sn}(\text{C}_4\text{H}_4\text{O}_6)$ in the liquid phase was turned continuously into the goal product SnO_2 in the solid phase rather than hydroxide.

3.4 Optical properties of the samples

For semiconductor materials, the band gap energy (E_g) is a key factor to the optical absorption properties. E_g can be estimated from the UV–Vis reflectance spectra using Tauc equation, $\alpha(\nu)h\nu = K(h\nu - E_g)^{n/2}$, where α is the optical absorption coefficient, k is an empirical constant, and $n = 1$ and 4 for direct and indirect band gaps [13], so the value of n is 1 for direct transition SnO_2 . Therefore, by plotting the curve of $(\alpha h\nu)^2$ versus $h\nu$ and extrapolating the curve to zero absorption coefficient, E_g can be obtained. As shown in Fig. 6a, the E_g of the calcinated $\text{SnO}_2:\text{xEu}$ ($x = 0.09$) samples is about 3.76 eV, which is higher than that (3.72 eV) of the sample without calcination. This is due to the increase in grain size after calcination [14]. From Fig. 6b, it can be observed that the E_g of undoped and Eu-doped SnO_2 samples is 3.80 and 3.76 eV, respectively. The relatively low E_g for Eu-doped SnO_2 sample results from the introduction of Eu^{3+} , which gives rise to structural defects, further creates allowed states lower than the conduction band energy levels [15], so E_g is decreased.

3.5 Luminescence properties of the samples

3.5.1 Excitation spectrum and emission spectrum of $\text{SnO}_2:\text{Eu}$

For the series of $\text{SnO}_2:\text{Eu}$ samples synthesized under different conditions, the profiles of excitation and emission spectra are similar. The $\text{SnO}_2:\text{xEu}$ ($x = 0.09$, $\text{pH} = 1$, $T = 900^\circ\text{C}$ and $t = 3$ h) sample is taken as an example. The excitation and emission spectra are shown in Fig. 7. It can be seen from Fig. 7a that the excitation spectrum (monitored at 589 nm) is composed of a broad band between 200 and 400 nm, which is attributed to the direct optical transition from the valence band to the conduction band in SnO_2 . The strongest peak is located at 323 nm, which is consistent with the band gap energy ($E_g = 3.76$ eV) of $\text{SnO}_2:\text{Eu}$ sample, therefore it is proved that the energy is transferred from the host to the luminescent centers.

As shown in Fig. 7b, the emission spectrum of the sample is consisted of a series of sharp peaks. The main emission peak at 589 nm is ascribed to the ${}^5\text{D}_0 \rightarrow {}^7\text{F}_1$ magnetic dipole transition of Eu^{3+} , and it splits into two peaks, which is attributed to the oxygen vacancies surrounding Eu^{3+} [16]. The series of weak emission peaks located at 608 ~ 633, 652 ~ 661 and ~ 720 nm are

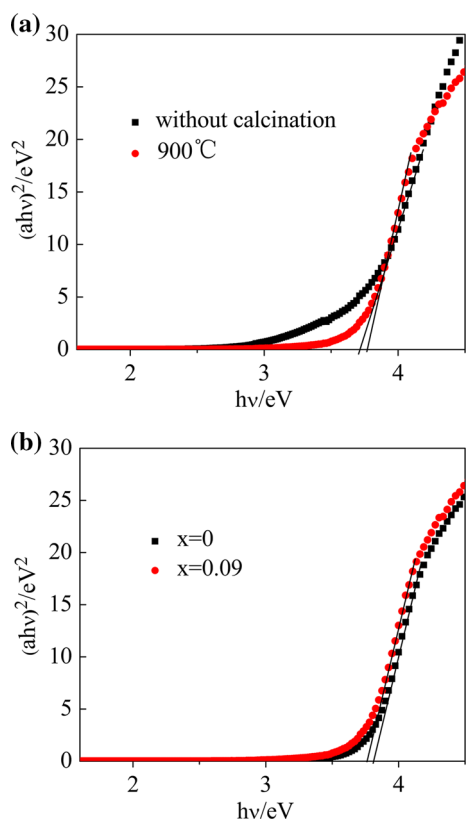


Fig. 6 Optical absorption spectra of samples obtained at **a** different calcination temperature ($x = 0.09$); **b** different Eu^{3+} concentration ($T = 900\text{ }^\circ\text{C}$)

assigned to the $^5\text{D}_0 \rightarrow ^7\text{F}_2$ (electric dipole transition), $^5\text{D}_0 \rightarrow ^7\text{F}_3$ and $^5\text{D}_0 \rightarrow ^7\text{F}_4$ transitions of Eu^{3+} respectively [17]. According to the selection rule, the magnetic dipole transition is allowed when the Eu^{3+} is located at the site with an inversion symmetric center, which leads to orange-red emitting around 590 nm [18]. As SnO_2 is tetragonal structure, in which Sn atom occupies an octahedral site, so the replacement of Sn^{4+} will produce high symmetric environment for Eu^{3+} . Thus, the magnetic dipole transition of Eu^{3+} is dominant in $\text{SnO}_2:\text{Eu}$ phosphors, while the electric dipole transition is relatively weak.

According to the above analysis, the possible energy transfer mechanism is presented in Fig. 7c. For a semiconductor, when irradiated with a light higher than or equal to the energy of E_g , electrons can be excited to the conduction band (CB), with the same amount of holes formed in the valence band (VB). Then the recombination of generated electrons and holes occurs due to electrostatic attraction, the energy is released and transferred to the luminescent centers Eu^{3+} . The excited electrons of Eu^{3+} get relax from $^5\text{D}_1 \rightarrow ^5\text{D}_0$ without photoemission [19]. The main electronic emission takes place between $^5\text{D}_0 \rightarrow ^7\text{F}_1$ at 589 nm wavelength.

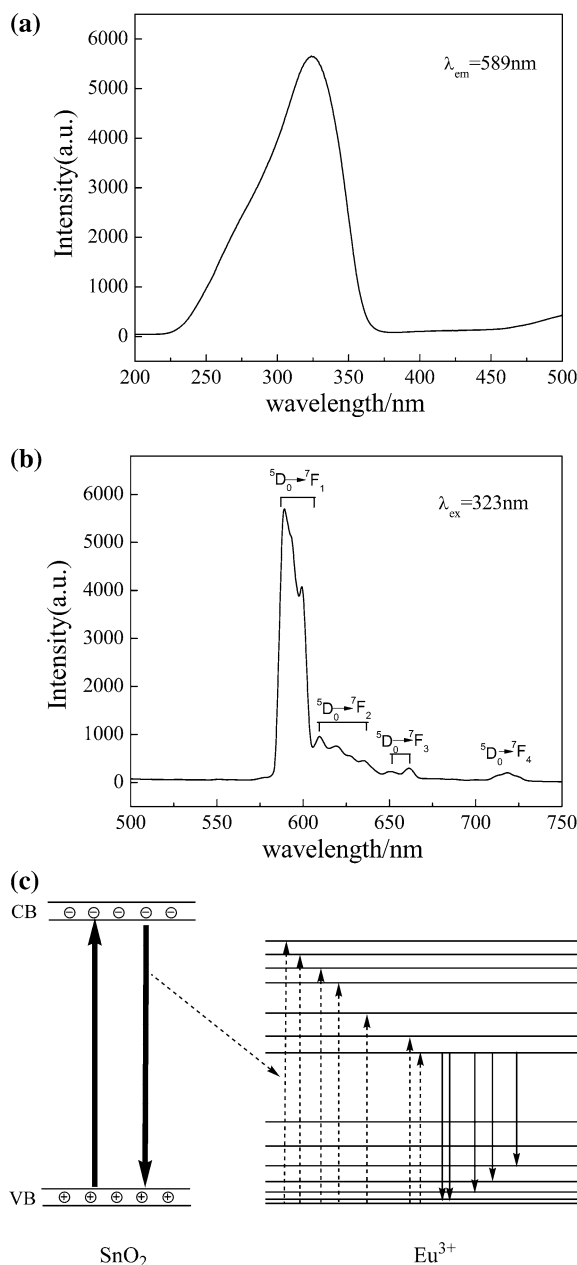


Fig. 7 Excitation **(a)** and emission **(b)** spectra of $\text{SnO}_2:\text{Eu}$; **c** the possible energy transfer mechanism between SnO_2 and Eu^{3+}

3.5.2 Influence of pH on luminescence properties of $\text{SnO}_2:\text{Eu}$

The emission spectra of $\text{SnO}_2:\text{Eu}$ samples synthesized under different pH are shown in Fig. 8. It can be seen that the pH has little effect on the position and shape of emission peaks, but has great effect on the intensity. When $\text{pH} = 1$, the peak intensity of the sample increases by about 400 % compared with the sample when $\text{pH} = 3$. According to the results of XRD analysis, the reason for this phenomenon is that the

sample is pure tetragonal phase $\text{SnO}_2:\text{Eu}$ with high crystallinity when $\text{pH} = 1$, but when the pH is increased to 3, some Eu^{3+} ions is changed into the impurity phase $\text{Eu}_2\text{Sn}_2\text{O}_7$ instead of replacing Sn^{4+} in SnO_2 host, which results in the decrease of luminescence centers, furthermore, the emission intensity becomes weaker. Therefore, the pH of solution can not only affect the phase of samples but also the luminescence performance.

3.5.3 Influence of calcination temperature on luminescence properties of $\text{SnO}_2:\text{Eu}$

Generally, the luminescence intensity of materials increases with calcination temperature due to grain growth and improved crystallinity. Figure 9 presents the emission spectra of $\text{SnO}_2:\text{Eu}$ obtained under different calcination temperature. It can be observed that the calcination temperature has significant effect on the intensity of emission peaks. The intensity of the main peak increases gradually with the increase of the calcination temperature from 700 to 900 °C, but when the calcination temperature is improved to 1000 °C, the intensity remains almost unchanged. This tendency is consistent with that of the crystallinity as the change of calcination temperature (shown in Fig. 2).

Among the characteristic emissions of Eu^{3+} , the ${}^5\text{D}_0 \rightarrow {}^7\text{F}_1$ magnetic dipole transitions are almost not affected by environmental changes while the ${}^5\text{D}_0 \rightarrow {}^7\text{F}_2$ electric dipole transitions are sensitive to the variation of local crystal field [20]. In order to illustrate the local distribution of Eu^{3+} in the SnO_2 lattice, the asymmetry ratio is introduced, which can be defined as $I({}^5\text{D}_0 \rightarrow {}^7\text{F}_2)/I({}^5\text{D}_0 \rightarrow {}^7\text{F}_1)$ [21]. The symmetry of local environment around Eu^{3+} increases with a decrease in the asymmetry ratio value. The grain size and asymmetry ratio of samples calcinated at different temperature are shown in Table 1. It can be seen that the grain size firstly increases with the increase of calcination temperature

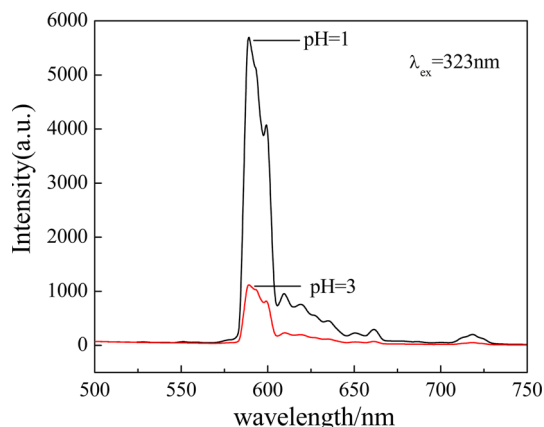


Fig. 8 Emission spectra of $\text{SnO}_2:\text{xEu}$ ($x = 0.09$) synthesized at different pH

then decreases in the range of 700 to 1000 °C. Accordingly, the asymmetry ratio value presents the opposite tendency. The sample calcinated at 900 °C has the largest size and the smallest asymmetry ratio, which indicates that the Eu^{3+} ions occupy highly symmetrical sites, this is beneficial to the orange–red emitting of $\text{SnO}_2:\text{Eu}$. So, 900 °C is selected as the optimum calcination temperature.

3.5.4 Influence of calcination time on luminescence properties of $\text{SnO}_2:\text{Eu}$

Calcination time can affect the crystallinity of the sample and the diffusion process of the activators in matrix, furthermore, affect the luminescent properties. Figure 10 shows the emission spectra of $\text{SnO}_2:\text{Eu}$ samples obtained under different calcination time. From these spectra, it can be seen that the intensity of emission peaks increases gradually along with the prolonged calcination time. From 1 to 3 h, the intensity of the main peak at 589 nm is increased by 25 %, while only 2 % from 3 to 5 h. This indicates that 3 h calcination time is adequate to gain the perfect crystallization and excellent luminescent properties.

3.5.5 Influence of Eu^{3+} doping concentration on luminescence properties of $\text{SnO}_2:\text{Eu}$

The concentration of activator determines the number of luminous center directly, furthermore, affects the luminescent properties. The emission spectra of $\text{SnO}_2:\text{xEu}$

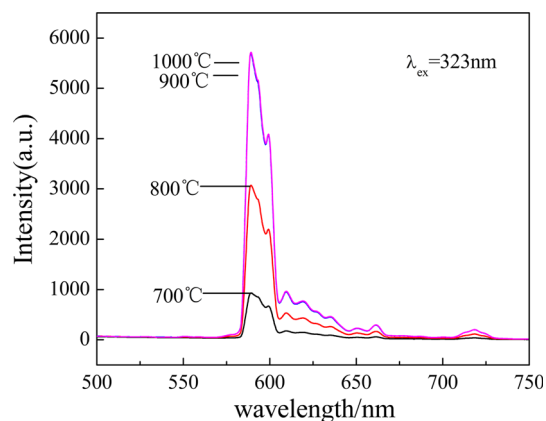


Fig. 9 Emission spectra of $\text{SnO}_2:\text{xEu}$ ($x = 0.09$) calcinated at different temperature

Table 1 Dependence of grain size and asymmetric ratio of samples on the calcination temperature

T (°C)	700	800	900	1000
Grain size (nm)	26	37	40	38
Asymmetric ratio	0.189	0.174	0.168	0.169

samples with different Eu^{3+} concentration (x) are presented in Fig. 11 (the inset is the curve of the emission intensity at 589 nm vs. x). It can be observed that the emission intensity at 589 nm of the sample firstly increases with the increase of Eu^{3+} concentration (x) from 0.03 to 0.09, and reaches the highest when $x = 0.09$, then decreases, which is due to the concentration quenching phenomenon. This is because when the Eu^{3+} concentration reaches a certain value, the interaction between Eu^{3+} ions increases and energy transfer generates, which results in the increase of the probability of non-radiative transitions [22], leading to the decrease of the emission intensity of Eu^{3+} . Moreover, when Eu^{3+} concentration is too high, excess oxygen defects formed in the host would destroy the crystallinity inevitably [23], which also results in the decrease of luminescent intensity. Therefore, $x = 0.09$ is the optimum doping concentration of Eu^{3+} .

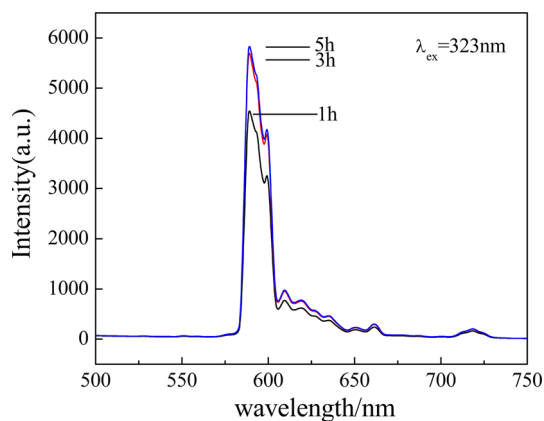


Fig. 10 Emission spectra of $\text{SnO}_2:\text{xEu}$ ($x = 0.09$) calcined for different time

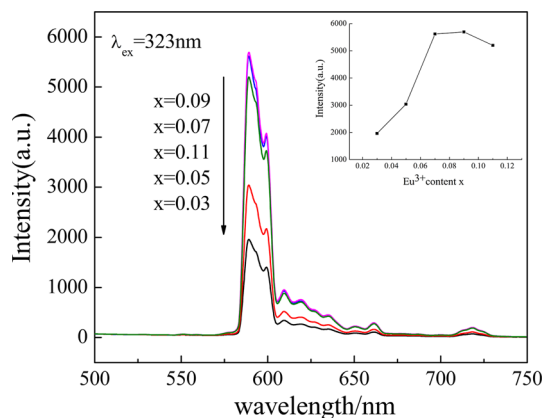


Fig. 11 Emission spectra of $\text{SnO}_2:\text{xEu}$ synthesized with different Eu^{3+} concentration

4 Conclusion

1. Nanosized $\text{SnO}_2:\text{Eu}$ phosphors were successfully synthesized by simple hydrothermal method followed by calcination process. The obtained samples were nearly spherical particles with a average size of 100 nm, possessed pure phase with high crystallinity and strong luminescent intensity. The appropriate reaction conditions were confirmed.
2. The strongest emission peak is located at 323 nm, which is consistent with the band gap energy ($E_g = 3.76$ eV) of $\text{SnO}_2:\text{Eu}$ sample, therefore it is proved that the energy is transferred from the host to the luminescent centers.
3. The high doping concentration of Eu^{3+} ($x = 0.09$) in SnO_2 matrix was achieved without impurity phase formation by the present synthesis route, so the luminescent intensity was enhanced significantly. The as-synthesized $\text{SnO}_2:\text{Eu}$ phosphor presented excellent orange–red-emitting properties with a broad excitation band, which made it a good candidate for potential orange–red-emitting phosphors used in the white LED.

Acknowledgments This study was supported by National Natural Science Foundation of China (No. 21301046).

References

1. Y. Guan, D.W. Wang, X. Zhou, P. Sun, H.Y. Wang, J. Ma, G.Y. Lu, *Sensor. Actuat. B-Chem.* **191**, 45 (2014)
2. A. Birkel, Y.G. Lee, D. Koll, X.V. Meerbeek, S. Frank, M.J. Choi, Y.S. Kang, K. Char, W. Tremel, *Energy Environ. Sci.* **5**, 5392 (2012)
3. H. Chen, L.F. Hu, X.S. Fang, L.M. Wu, *Adv. Funct. Mater.* **22**, 1229 (2012)
4. Y.C. Chang, C.Y. Yan, R.J. Wu, *J. Chin. Chem. Soc.* **61**, 345 (2014)
5. S. Sambasivam, S.B. Kim, J.H. Jeong, B.C. Choi, K.T. Lim, S.S. Kim, T.K. Song, *Curr. Appl. Phys.* **10**, 1383 (2010)
6. J.C. Zhang, X.L. Ma, Q.S. Qin, L.R. Shi, J.Y. Sun, M.J. Zhou, B.T. Liu, Y.H. Wang, *Mater. Chem. Phys.* **136**, 320 (2012)
7. S.K. Pillai, L.M. Sikhivihilu, T.K. Hillie, *Mater. Chem. Phys.* **120**, 619 (2010)
8. X.Y. Fu, H.W. Zhang, S.Y. Niu, Q. Xin, *J. Solid State Chem.* **178**, 603 (2005)
9. X.Y. Fu, S.Y. Niu, H.W. Zhang, Q.W. Min, Q. Xin, *Mater. Sci. Eng. B* **123**, 45 (2005)
10. P. Psuja, W. Streck, *J. Rare Earths* **30**, 627 (2012)
11. R.S. Ningthoujam, V. Sudarsan, S.K. Kulshreshtha, *J. Lumin.* **127**, 747 (2007)
12. H.W. Zhang, X.Y. Fu, S.Y. Niu, G.Q. Sun, Q. Xin, *J. Lumin.* **115**, 7 (2005)
13. Y.I. Choi, Y.K. Sohn, *RSC Adv.* **4**, 31155 (2014)
14. R. Singh, M. Kumar, S. Shankar, R. Singh, A.K. Ghosh, O.P. Thakur, B. Das, *Mater. Sci. Semicon. Proc.* **31**, 310 (2015)
15. R.K. Mishra, P.P. Sahay, *Mater. Res. Bull.* **47**, 4112 (2012)
16. J.T. Chen, J. Wang, F. Zhang, D. Yan, G.A. Zhang, R.F. Zhuo, P.X. Yan, *J. Phys. D Appl. Phys.* **41**, 105306 (2008)

17. H. Guo, Y.M. Qiao, *Appl. Surf. Sci.* **254**, 1961 (2008)
18. Y.Q. Zhai, Z.J. You, Y.H. Liu, Y.P. Sun, Q.Q. Ji, *J. Rare Earths* **30**, 114 (2012)
19. A.U. Pawar, A.P. Jadhav, U. Pal, B.K. Kim, Y.S. Kang, *J. Lumin.* **132**, 659 (2012)
20. A.P. Jadhav, A.U. Pawar, U. Pal, Y.S. Kang, *J. Mater. Chem. C* **2**, 496 (2014)
21. R.S. Ningthoujam, V. Sudarsan, S.V. Godbole, L. Kienle, S.K. Kulshreshtha, A.K. Tyagi, *Appl. Phys. Lett.* **90**, 173113 (2007)
22. B. Han, J. Zhang, Z.M. Wang, Y.Y. Liu, H.Z. Shi, *J. Lumin.* **149**, 150 (2014)
23. L.D. Sun, C. Qian, C.S. Liao, X.L. Wang, C.H. Yan, *Solid State Commun.* **119**, 393 (2001)